HU sensitivity

To examine cellular sensitivity to HU, growing cells were washed once with SFM and treated with the complete culture medium containing 2 mM HU (Wako Pure Chemical Industries, Osaka) for 24 h. Then the cells were replated into 100-mm dishes and cultured with the complete culture medium for 14 days. Colonies more than 50 cells were scored as survivors.

Chromosome aberrations induced with X-rays at G_2 phase

To examine chromosome aberrations induced with X-rays at G_2 phase, exponentially growing cells were irradiated with 1 Gy of X-rays using an X-ray generator (M-150 WE; Softex, Osaka) operating at 150 kVp and 5 mA with a 0.1 mm Cu filter at a dose rate of 0.425 Gy/min, treated with Colcemid (60 ng/ml) for 2 h, and harvested. Chromosome samples were prepared as described above and stained with 5% Giemsa solution for 10 min. One hundred metaphases for each cell strain were scored for chromatid gaps and breaks.

RESULTS

Presence of an extra chromosome 8 in the microcell hybrid cells

Microcell fusion experiments were tried six times to introduce a human chromosome 8 containing a normal *WRN* gene into h*TERT*-immortalized WS3RGB/T cells. Average number of recipient cells assayed for one trial of the chromosome transfer was 2.0×10^6. We finally obtained one microcell hybrid that acquired blasticidin S resistance and designated it as WS3RGB/T-8, of which frequency for chromosome transfer was 8.3×10^{-8}. To confirm the presence of an extra copy of chromosome 8 in the microcell hybrid, we examined the copy number of chromosome 8 using whole chromosome painting by scoring 100 metaphases each in parental WS3RGB/T cells and WS3RGB/T-8 cells (Table 1 and Fig. 1). In the parental WS3RGB/T cells, all metaphases (100%) had two copies of chromosome 8; one was intact and the other was translocated to another chromosome (Fig. 1A). In contrast to this, all metaphases (100%) retained an extra copy of intact chromosome 8 in WS3RGB/T-8 cells (Fig. 1B), confirming a successful transfer of a chromosome 8.

Expression of the WRN gene and protein

To examine the expression of the *WRN* gene in WS3RGB/T-8 cells, we used RT-PCR to amplify cDNAs for the *WRN* gene and the *c-myc* gene in BJ/hTERT cells, WS3RGB/T cells and WS3RGB/T-8 cells. We adopted *c-myc* gene as a control for gene expression because its expression was relatively constant through cell cycle[18] and its gene dosage was the same as that of the *WRN* gene based on the fact that both

Table 1. Chromosome analyses in WS3RGB/T cells and WS3RGB/T-8 cells

Cell	Introduced chromosome	No. of metaphases scored	Percentage of cells with the extra chromosome 8	Morphology of the extra chromosome 8
WS3RGB/T	–	100	–	–
WS3RGB/T-8	8	100	100	Intact

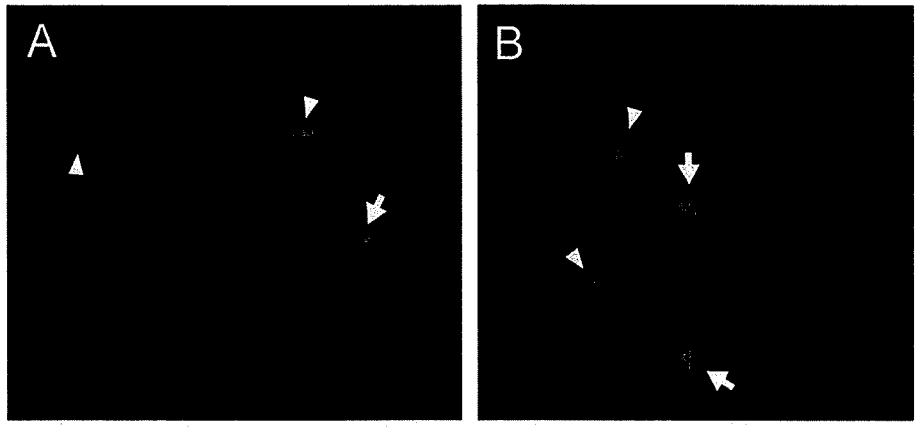

Fig. 1. The presence of an extra copy of chromosome 8 in microcell hybrid WS3RGB/T-8 cells. Metaphase spreads of (A) parental WS3RGB/T cells and (B) WS3RGB/T-8 cells are represented. The presence of an extra copy of chromosome 8 in WS3RGB/T-8 cells was confirmed by whole chromosome painting using a probe specific for chromosome 8. Arrows, an intact chromosome 8; Arrowheads, a rearranged chromosome 8.

genes located on chromosome 8. As shown in Fig. 2, the expression of the *WRN* gene in WS3RGB/T cells was very low, showing 4% level of that in the control BJ/hTERT cells (Fig. 2B), although those two types of cells expressed the *c-myc* gene at similar levels. In contrast, the expression of the *WRN* gene in WS3RGB/T-8 cells shows 48% level of that in the control cells (Fig. 2B). These results were consistent with those obtained by Western blotting, where the expression of the WRN protein was 6% and 52% level of that in the control cells in WS3RGB/T cells and in WS3RGB/T-8 cells, respectively (Fig. 3A and 3B).

Sensitivities to 4NQO and HU

To examine functional complementation of WS phenotypes by the expression of the *WRN* gene, we determined the sensitivities to 4NQO and HU in BJ/hTERT cells, WS3RGB/T cells, and WS3RGB/T-8 cells. As shown in Fig. 4, WS3RGB/T cells were more sensitive to 4NQO than the control (BJ/hTERT) cells. In contrast, the expression of the *WRN* gene conferred resistance to 4NQO in WS3RGB/T-8 (Fig. 4). Similarly, although WS3RGB/T cells were hypersensitive to 2mM HU as compared with the control cells ($p < 0.01$, Student's t-test), the expression of the *WRN* gene recovered resistant to HU ($p < 0.05$, Student's t-test) in WS3RGB/T-8 cells as shown in Fig. 5. These results indicate that the expression of *WRN* gene in the immortalized WS cell line (WS3RGB/T-8) can complement the WS phenotypes such as the hypersensitivities to 4NQO and HU.

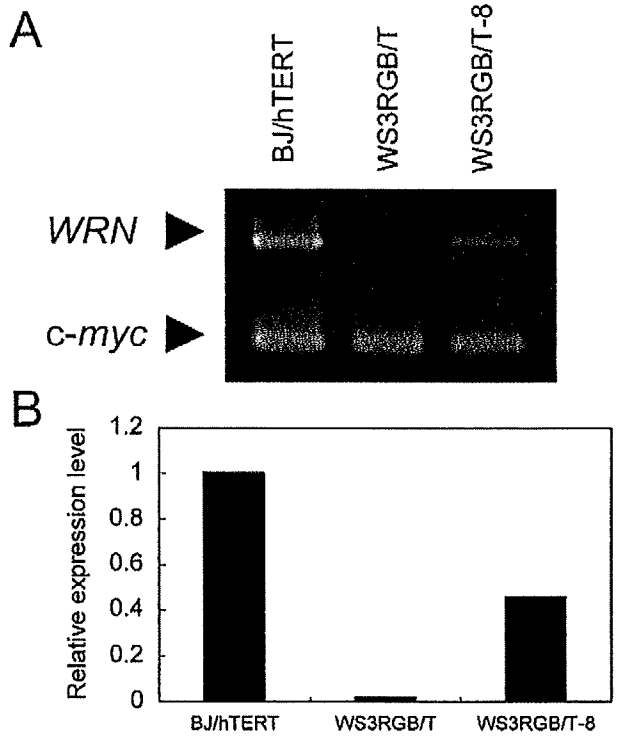

Fig. 2. Expression of the *WRN* gene in WS3RGB/T cells and WS3RGB/T-8 cells. (A) The expression levels of the *WRN* gene and the c-*myc* gene were measured by RT-PCR. Cells used were BJ/hTERT (a human control cell line), WS3RGB/T, and WS3RGB/T-8. (B) The relative expression of the *WRN* gene was determined as described in Material and Methods.

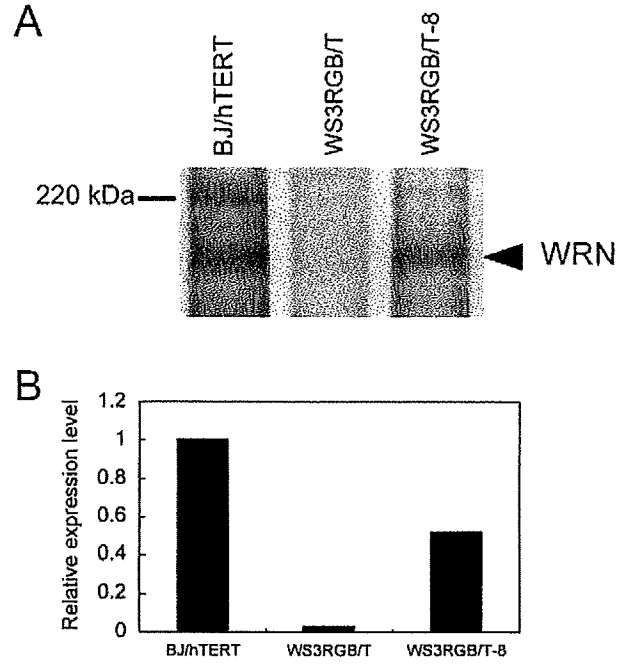

Fig. 3. Western blot analysis of the WRN protein. (A) The expression level of the WRN protein was measured by Western blotting. Cells used were BJ/hTERT, WS3RGB/T, and WS3RGB/T-8. (B) The relative expression of the WRN protein was determined as described in Material and Methods.

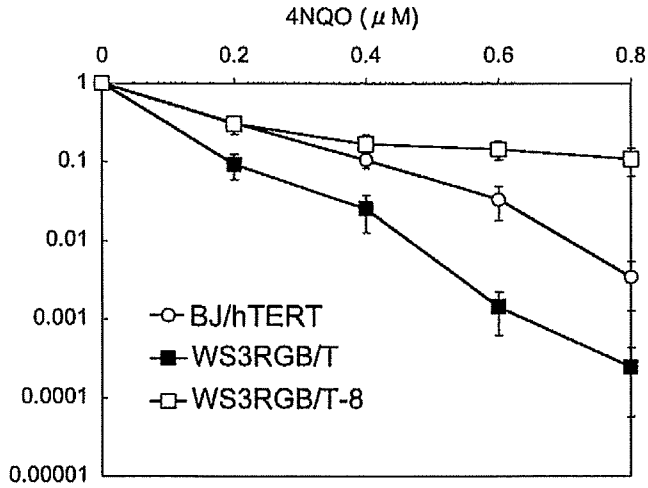

Fig. 4. Sensitivity to 4NQO assayed by colony-forming ability. Cells examined were BJ/hTERT (○), WS3RGB/T (■), and WS3RGB/T-8 (□). The cells were treated with 4NQO for 1 h and incubated for 2 weeks for colony formation.

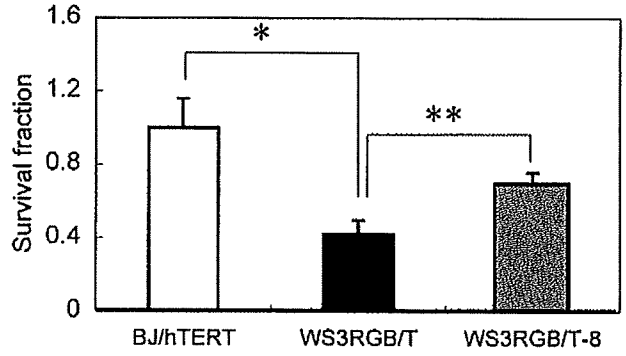

Fig. 5. Sensitivity to HU assayed by colony-forming ability. Cells examined were BJ/hTERT, WS3RGB/T, and WS3RGB/T-8. The cells were treated with 2 mM HU for 24 h and incubated for 2 weeks for colony formation. The differences are significant by Student's t-test (*$p < 0.01$, **$p < 0.05$).

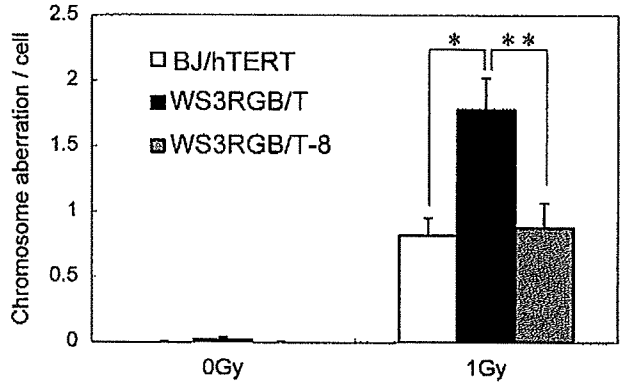

Fig. 6. Chromosome aberrations induced by X-irradiation at G_2 phase. Cells examined were BJ/hTERT (white bar), WS3RGB/T (black bar), and WS3RGB/T-8 (gray bar). The cells were irradiated with 1 Gy of X-rays and one hundred metaphases for each cell strain were scored for chromatid gaps and breaks. The differences are significant by Welch's t-test (*$p < 0.01$, **$p < 0.05$).

Chromosomal sensitivity to ionizing radiation at G_2 phase

We selected chromosomal sensitivity to ionizing radiation at G_2 phase as a WS phenotype[13] to be examined the complementation by the WRN expression. As shown in Fig. 6, WS3RGB/T cells showed a higher frequency of chromosome aberrations than the control cells after exposure to 1 Gy of X-rays at G_2 phase ($p < 0.01$, Welch's t-test). In contrast to this, the frequency of chromosome aberrations in WS3RGB/T-8 cells was reduced to the level as low as that of the control cells ($p < 0.05$, Welch's t-test). The result indicates that the expression of the *WRN* gene can correct the abnormal chromosomal sensitivity to ionizing radiation at G_2 phase observed in WS cells.

DISCUSSION

We demonstrated that the expression of the WRN protein corrects the abnormal WS phenotypes in an immortalized WS cell line. The corrected WS phenotypes are cellular sensitivities to 4NQO[7,8] and HU,[12] and chromosomal radiosensitivity at G_2 phase. This is contrast to the results reported in our previous study,[14] where we failed to complement the abnormal WS phenotypes such as the hypersensitivity to 4NQO and high proportion of deletion mutations at *HPRT* locus by the expression of the *WRN* gene. However, in the present study, we could not determine the mutation types at *HPRT* locus for confirming that spontaneous deletion mutations occur in a high proportion in WS cells, which was well characterized and one of the most interesting cellular phenotype of WS cells.[14–16] Because WS3RGB/T cells used in the present study were female origin in contrast to WS780 cells, which were male origin and used in the previous study, the detection of mutation at *HPRT* locus was not possible in WS3RGB/T cells.

In both previous and present studies, we adopted the same chromosome transfer method to complement the defect of WS phenotypes, but the recipient WS cells were different between two studies. Whereas we used a SV40-immortalized WS cell line (WS780) in the previous study, we adopted an h*TERT*-immortalized WS cell line (WS3RGB/T) in the present study. We do not have a clear answer to explain the reason why we could not correct the WS phenotypes in the SV40-immortalized WS cells in the previous study. A possible answer is that the SV40-immortalized cells are genetically unstable as compared with those immortalized by the h*TERT* gene so that multiple mutations are accumulated during the establishment of cell line. These secondary mutations might be involved in the failure of complementing the WS phenotypes. Therefore, it is not recommendable to use SV40-immortalized human cells to examine the complementation of mutant phenotypes because secondary mutations that might be accumulated in those cells may hamper the function of gene product that is asked. In contrast, as demonstrated in the present study, h*TERT*-immortalized human cells are more stable than SV40-immortalized human cells and useful for examining the complementation test.

In terms of the sensitivities to 4NQO and HU, it turned out in the present study that the WRN function is primarily, but not secondarily, involved in the recovery of resistance to 4NQO and HU. 4NQO induces a spectrum of DNA and chromatin lesions including oxidative DNA damage, single-strand breaks, base intercalations, adducts, and cross-links. There has been no direct evidence to indicate that the WRN protein plays a critical role in the repair process of those lesions. However, evidence has been accumulated to show that WS cells are hypersensitive to DNA cross-linking agents such as mitomycin C (MMC) and *cis*-platinum (II)

diamine dichloride (CDDP),[11] suggesting that the WRN protein might participate in the resolution of DNA cross-link damage induced by 4NQO. Another possibility of the 4NQO hypersensitivity in WS cells is due to a defective response to oxidative damage induced by 4NQO because a recent study[19] indicates that knockdown of the WRN expression using RNA interference (RNAi) in primary human fibroblast cells accelerates cellular senescence and accumulation of DNA double-strand breaks caused by oxidative stress. Furthermore, *in vivo* oxidative stress has been shown to be elevated in both WS patients and mutant mice of the mouse *WRN* gene.[20–22] These studies implicate a significant role of the WRN protein in dealing with DNA damage delivered by oxidative stress.

Several lines of evidence suggest a role of the WRN protein in DNA replication. For example, WS cells show extended S-phase[23] and reduced frequency of replication initiation sites compared with normal cells.[24,25] In addition, the WRN protein interacts with RPA protein that is required for replication,[26] and co-localizes with RPA upon replication fork arrest after HU treatment.[27] These results, together with a report demonstrating the requirement of the WRN protein for correct recovery after replication arrest,[12] suggest a significant role of the WRN protein in DNA replication. The evidence that the HU hypersensitivity in WS cells can be corrected by the expression of the WRN protein (Fig. 5) indicates that this abnormal WS phenotype is also caused primarily by a defect of the WRN function.

Although WS has not been categorized as a DNA repair-deficient genetic disease, there has been some reports to suggest that the WRN protein participates in repairing radiation-induced DNA damage. For example, we previously demonstrated that exogenous expression of exonuclease domain-deleted WRN protein in human 293 cells increased radiosensitivity in terms of cell survival and chromosome aberrations,[17] suggesting that a function of WRN exonuclease activity is essential for the repair of radiation-induced DNA damage. Also, Yannone *et al.* demonstrated that WS cells immortalized by the h*TERT* gene were radiosensitive and that this hypersensitivity was complemented by introduction of the *WRN* gene.[28] In addition to these, WS cells were characterized by an abnormal radiation response at G_2 phase.[13] These findings are consistent with our present result that the frequency of X-ray-induced chromosome aberrations at G_2 phase in WS3RGB/T cells was significantly higher than that of the control cells (Fig. 6), suggesting that DNA damage response induced by ionizing radiation at G_2 phase is defected in WS3RGB/T cells. The evidence that chromosomal radiosensitivity is completely normalized in WS3RGB/T-8 suggests that normal DNA damage response at G_2 phase requires the WRN function.

It should be noticed that the abnormal phenotypes in the 4NQO sensitivity (Fig. 4) and the chromosomal radiosensitivity at G_2 phase (Fig. 6) in WS3RGB/T cells are fully recovered in WS3RGB/T-8 cells even though the expression level of the WRN protein is almost half compared with that of the control cells as shown in Fig. 3. This implies that a half expression level of the WRN protein is enough to recover from the phenotypic defects observed in WS cells. The result is consistent with the fact that WS heterozygotes are phenotipically indistinguishable from normal individuals.

In summary, the present study demonstrated that the expression of the *WRN* gene complements abnormal WS phenotypes, i.e., the hypersensitivities to some types of DNA or chromatin lesion and DNA replication arrest, and also the abnormal response to ionizing radiation at G_2 phase, in h*TERT*-immortalized WS cells. This indicates that those multiple abnormal phenotypes are derived from a primary, but not secondary, defect in the *WRN* gene. In addition, the present study clearly indicates that h*TERT*-immortalized human cells are better than SV40-immortalized human cells to use in the complementation study.

ACKNOWLEDGEMENTS

This work was partly supported by a Grant-in Aid for Scientific Research from the Ministry of Education, Culture, Sports, Science and Technology of Japan.

REFERENCES

1. Salk, D. (1982) Werner's syndrome: a review of recent research with an analysis of connective tissue metabolism, growth control of cultured cells, and chromosomal aberrations. Hum. Genet. **62**: 1–5.
2. Martin, G. M., Oshima, J., Gray, M. D. and Poot, M. (1999) What geriatricians should know about the Werner syndrome. J. Am. Geriatr. Soc. **47**: 1136–1144.
3. Yu, C. E., Oshima, J., Fu, Y. H., Wijsman, E. M., Hisama, F., Alisch, R., Matthews, S., Nakura, J., Miki, T., Ouais, S., Martin, G. M., Mulligan, J. and Schellenberg, G. D. (1996) Positional cloning of the Werner's syndrome gene. Science **272**: 258–262.
4. Gray, M. D., Shen, J. C. Kamath-Loeb, A. S., Blank, A., Sopher, B. L., Martin, G. M., Oshima, J. and Loeb, L. A. (1997) The Werner syndrome protein is a DNA helicase, Nat. Genet. **17**: 100–103.
5. Huang, S., Li, B., Gray, M. D., Oshima, J., Mian, I. S. and Campisi, J. (1998) The premature ageing syndrome protein, WRN, is a 3'→5' exonuclease. Nat. Genet. **20**: 114–116.
6. Brosh, R. M. and Bohr, V. A. (2007) Human premature aging, DNA repair and RecQ helicases. Nuc. Acids Res. **22**: 7527–7544.
7. Ogburn, C. E., Oshima, J., Poot, M., Chen, R., Hunt, K. E. Gollahon, K. A., Rabinovitch, P. S. and Martin, G. M. (1997) An apoptosis-inducing genotoxin differentiates heterozygotic carriers for Werner helicase mutations from wild-type and homozygous mutants. Hum. Genet. **101**: 121–125.
8. Poot, M., Gollahon, K. A., Emond, M. J., Silber, J. R. and Rabinovitch, P. S. (2002) Werner syndrome diploid fibroblasts are sensitive to 4-nitroquinoline-N-oxide and 8-

methoxypsoralen: implications for the disease phenotype. FASEB J. **16**: 757–758.
9. Label, M. and Leder, P. (1998) A deletion within the murine Werner syndrome helicase induces sensitivity to inhibitors of topoisomerase and loss of cellular proliferative capacity. Proc. Natl. Acad. Sci. USA. **95**: 13097–13102.
10. Poot, M., Gollahon, K. A. and Rabinovitch, P. S. (1999) Werner syndrome lymphoblastoid cells are sensitive to camptothecin-induced apoptosis in S-phase. Hum. Genet. **104**: 10–14.
11. Poot, M., Yom, J. S., Whang S. H., Kato, J. T., Gollahon, K. A. and Rabinovitch, P. S. (2001) Werner syndrome cells are sensitive to DNA cross-linking drugs. FASEB J. **15**: 1224–1226.
12. Pichierri, P., Franchitto, A., Mosesso, P. and Palitti, F. (2001) Werner's syndrome protein is required for correct recovery after replication arrest and DNA damage induced in S-phase of cell cycle. Mol. Biol. Cell, **12**: 2412–2421.
13. Franchitto, A., Proietti, De Santis, L., Pichierri, P., Mosesso, P. and Palitti, F. (1999) Lack of effect of caffeine post-treatment on X-ray-induced chromosomal aberrations in Werner's syndrome lymphoblastoid cell lines: a preliminary report. Int. J. Radiat. Biol. **75**: 1349–1355.
14. Kodama, S., Kashino, G., Suzuki, K., Takatsuji, T., Okumura, Y., Oshimura, M., Watanabe, M. and Barrett, J. C. (1998) Failure to complement abnormal phenotypes of simian virus 40-transformed Werner syndrome cells by introduction of a normal human chromosome 8. Cancer Res. **58**: 5188–5195.
15. Fukuchi, K., Martin, G. M. and Monnat, R. J. Jr. (1989) Mutator phenotype of Werner syndrome is characterized by extensive deletions. Proc. Natl. Acad. Sci. USA. **86**: 5893–5897.
16. Oshima, J., Huang, S., Pae, C., Campisi, J. and Schiestl, R. H. (2002) Lack of WRN results in extensive deletion at nonhomologous joining ends. Cancer Res. **62**: 547–551.
17. Kashino, G., Kodama, S., Suzuki, S., Matsumoto, T. and Watanabe, M. (2005) Exogenous expression of exonuclease domain-deleted WRN interferes with the repair of radiation-induced DNA damages. J. Radiat. Res. **46**: 407–414.
18. Gazitt, Y. and Erdos, G. W. (1994) Fluctuation and ultrastructural localization of oncoproteins and cell cycle regulatory protein during growth and apoptosis of synchronized AGF cells. Cancer Res. **54**: 950–956.
19. Szekely, A. M., Bleichert, F., Numann, A., Van Komen, S., Manasanch, E., Ben Nasr, A., Canaan, A. and Weissman, S. M. (2005) Werner protein protects nonproliferating cells from oxidative DNA damage. Mol. Cell Biol. **25**: 10492–10506.
20. Pagano, G., Zatterale, A., Degan, P., d'Ischia, M., Kelly, F. J., Pallardo, F. V. and Kodama, S. (2005) Multiple involvement of oxidative stress in Werner syndrome phenotype. Biogerontology. **6**: 233–243.
21. Pagano, G., Zatterale, A., Degan, P., d'Ischia, M., Kelly, F. J., Pallardo, F. V., Calzone, R., Castello, G., Dunster, C., Giudice, A., Kilinc, Y., Lloret, A., Manini, P., Masella, R., Vuttariello, E. and Warnau, M. (2005) *In vivo* prooxidant state in Werner syndrome (WS): results from three WS patients and two WS heterozygotes. Free Radic. Res. **39**: 529–533.
22. Massip, L., Garand, C., Turaga, R. V., Deschenes, F., Thorin, E. and Lebel, M. (2005) Increased insulin, triglycerides, reactive oxygen species, and cardiac fibrosis in mice with a mutation in the helicase domain of the Werner syndrome gene homologue. Exp. Gerontol. **41**: 157–168.
23. Poot, M., Hoehn, H., Runger, T. M. and Martin, G. M. (1992) Impaired S-phase transit of Werner syndrome cells expressed in lymphoblastoid cells. Exp. Cell Res. **202**: 267–273.
24. Takeuchi, F., Hanaoka, F., Goto, M., Akaoka, I., Hori, T., Yamada, M. and Miyamoto, T. (1982) Alterd frequency of initiation sites of DNA replication in Werner's syndrome cells. Hum. Genet. **60**: 365–368.
25. Hanaoka, F., Yamada, M., Takeuchi, F., Goto, M., Miyamoto, T. and Hori, T. (1985) Autoradiographic studies of DNA replication in Werner's syndrome cells. Adv. Exp. Med. Biol. **190**: 439–457.
26. Wold, M. S. (1997) Replication protein A: a heterotrimeric, single-stranded DNA-binding protein required for eukaryotic DNA metabolism. Annu. Rev. Biochem. **66**: 61–92.
27. Constantinou, A., Tarsounas, M., Karow, J. K., Brosh, R. M., Bohr, V. A., Hickson, I. D. and West, S. C. (2000) Werner's syndrome protein (WRN) migrates Holliday junctions and co-localizes with RPA upon replication arrest. EMBO Rep. **1**: 80–84.
28. Yannone, S. M., Roy, S., Chau, D. W., Murphy, H. B., Huang, S., Campisi, J. and Chen, D. J. (2001) Werner syndrome protein is regulated and phosphorylated by DNA dependent protein kinase. J. Biol. Chem. **276**: 38242–38248.

Received on November 4, 2008
Revision received on March 9, 2009
Accepted on March 16, 2009
J-STAGE Advance Publication Date: April 25, 2009

J. Radiat. Res., 50: Suppl., A29-A47 (2009)

Microbeam Irradiation Facilities for Radiobiology in Japan and China

Yasuhiko KOBAYASHI[1,2,3], Tomoo FUNAYAMA[3], Nobuyuki HAMADA[1,2,3,10], Tetsuya SAKASHITA[3], Teruaki KONISHI[4], Hitoshi IMASEKI[4], Keisuke YASUDA[5], Masanori HATASHITA[5], Keiichi TAKAGI[5], Satoshi HATORI[5], Keiji SUZUKI[6], Motohiro YAMAUCHI[6], Shunichi YAMASHITA[6], Masanori TOMITA[7], Munetoshi MAEDA[7,8], Katsumi KOBAYASHI[8*], Noriko USAMI[8] and Lijun WU[9]

Heavy-ion microbeam/Light-ion microbeam/X-ray microbeam/Bystander effects/Nucleus irradiation/Cytoplasm irradiation.

In order to study the radiobiological effects of low dose radiation, microbeam irradiation facilities have been developed in the world. This type of facilities now becomes an essential tool for studying bystander effects and relating signaling phenomena in cells or tissues. This review introduces you available microbeam facilities in Japan and in China, to promote radiobiology using microbeam probe and to encourage collaborative research between radiobiologists interested in using microbeam in Japan and in China.

INTRODUCTION

Biological effect of low dose radiation has been attracted much attention in modern human society, not only due to high dependence to nuclear power as energy source, but also due to realization of human activity in space. In order to investigate mechanisms of biological effects, heterogeneity of radiation dose in cellular level became a big barrier to be overcome. This heterogeneity becomes apparent in relatively higher dose in high LET, heavy-particle irradiation than in low LET, electron or photon irradiation. From this rational, microbeam irradiation facilities using proton or He ion were developed in 1990s in Gray laboratory, UK[1)] and in Columbia University, USA.[2)] Their pioneering works revealed various interesting results concerning heterogeneous distribution of dose, or particle traversal per cell. Also demonstrated in the reports are non-targeted effects, or bystander effects, which was found as effects observed in cells not directly hit or irradiated, but situated nearly the cells actually received the radiation. As conventional radiation biology is based on the premise that only those cell nuclei exposed to radiation treatment are affected, the presence of bystander effects forces a paradigm shift and reevaluation of modern radiation biology.

So far, two types of micro irradiation facilities have been developed widely in the world, one of which is high-LET particle microbeam irradiation, and the other is soft X-ray or X-ray microbeam irradiation. Several important evidences have been discovered that have never been described in the study using conventional irradiation. For example, the studies have found that there is a mechanism to transport bystander signals between the targeted cells and neighboring untargeted cells through gap-junctional intercellular communication.[3)] It was also shown that a single hit cell among thousands of cells could induce bystander effects, indicating that there are soluble factors, secreted from the targeted cells, which mediate non-targeted effects.[4,5)] Moreover, nuclear micro-irradiation as well as cytoplasmic micro-irradiation initiates bystander effects, implicating that not

*Corresponding author: Phone: +81-29-864-5655,
Fax: +81-29-864-2801,
E-mail: katsumi.kobayashi@kek.jp
[1]Department of Quantum Biology, Division of Bioregulatory Medicine, Gumma Univ. Graduate School of Medicine, Maebashi, Gumma 371-8511, Japan; [2]The 21st Century Center of Excellence (COE) Program for Biomedical Research Using Accelerator Technology; [3]Microbeam Radiation Biology Group, Radiation-Applied Biology Division, Quantum Beam Science Directorate, Japan Atomic Energy Agency (JAEA), Takasaki, Gunma 370-1292, Japan; [4]Dept. Technical Support and Development, National Institute of Radiological Sciences, Chiba, Chiba 263-8555, Japan; [5]The Wakasa Wan Energy Research Center, Tsuruga, Fukui 914-0192, Japan; [6]Atomic Bomb Disease Institute, Graduate School of Biomedical Sciences, Nagasaki University, Nagasaki, Nagasaki 852-8521, Japan; [7]Cenral Research Institute of Electric Power Industry, Komae, Tokyo 201-8511, Japan; [8]Photon Factory, KEK, Tsukuba, Ibaraki 305-0801, Japan; [9]Key Laboratory of Ion Beam Bioengineering, Hefei, Anhui 230031, China; [10]Present address: Dept. Pathology, Institute of Development, Aging and Cancer, Tohoku Univ. Sendai 980-8575, Japan.
doi:10.1269/jrr.09009S

List of microbeam facilities for radiobiology in Japan and China

Institute or University	Location	Type of Beam and Its Energy	MinimunBeamSize
TIARA, Japan Atomic Energy Agency	Takasaki, Japan	C (18.3 MeV/u), Ne(17.5 MeV/u), Ar(11.5 MeV/u)	5 μm
SPICE, National Institue of Radiological Science	Chiba, Japan	proton, 3.4 MeV	5 μm
Wakasa Wan Energy Research Center	Tsuruga, Japan	proton(10 MeV), He (15MeV)	10 μm
Nagasaki University	Nagasaki, Japan	ultrasoft X-rays, 0.25 keV	a few μm
Central Research Institute of Elec. Power Ind.	Tokyo, Japan	soft X-rays, 1.49 keV	2 μm
Photon Factory, KEK	Tsukuba, Japan	X-rays, 4 - 20 keV	5 μm
Key Lab. Ion Beam Bioengineering(LIBB)	Hefei, China	proton, 2-3 MeV	5 μm

only DNA damage but also dysfunction of mitochondria plays a role in generating bystander signals.[6,7] It is quite clear that these findings have never been discovered without targeted micro irradiation, and thus, microbeam irradiation becomes indispensable for studying such non-targeted effects.

Soon after the construction of microbeam irradiation facilities for raidiobiology in UK and USA, a project of microbeam irradiation using heavy ions started in JAEA, Takasaki in Japan. These facilities provided concrete evidence on bystander effects and related phenomena, which turned on the explosive progress in radiobiology in low dose region. Since then, several proposals for constructing microbeam irradiation systems have been proposed in Japan, and presently six systems are working and some more, under development or being planned. One of the characteristics in microbeam research status in Japan is that various types of radiation are available, including soft X-rays, X-rays, light ions and heavy ions. This indicates a potentiality of explosive development in microbeam radiobiology in Japan. This review introduces present status and characteristics of these six microbeam facilities, all of which are open to outside users under some sort of collaboration programs, in order to encourage Japanese radiobiologists for using them and to promote radiobiology in Japan. For the convenience of readers, characteristics of these facilities are summarized in one Table. Also added in this review is a microbeam facility in Hefei, China, since China is not so far located for the collaboration of Japanese scientists.

HEAVY-ION MICROBEAM SYSTEM AT JAEA-TAKASAKI FOR BIOLOGICAL STUDIES

Introduction

Advantage associated with the use of heavy-ion microbeam irradiation concerns the precise detection of ion-hit position on micron-scale targets. According to the model of ion track structure, track structure of heavy ions is characterized by a higher ionization density in the central part of the track, called "core", and a larger diameter of secondary electrons called "penumbra" or "delta rays", but the range of energy deposition is no more than a few micrometers. On the other hand, cell nuclei range from ten up to several tens of micrometers in size. Therefore, when investigating biological effects together with the relationship to ion track structure, it is important to know the precise position where ion(s) hit. A precise regulation of the target position on the cell nucleus by microbeam irradiation makes it possible to obtain the information on the position of ion traversal and on cellular responses induced by ion hit simultaneously, indicating microbeam is an operative means for elucidating initial cellular responses together with the relationship with ion track structure.

Heavy ion-induced bystander effect is a phenomenon that may be of concern to astronauts exposed to space radiation during long-term space missions.[8,9] On this context, the use of heavy-ion microbeam is important for assessing health risk of space radiation.

The use of heavy-ion microbeams has not been restricted to the area of radiation biology and has been applied to other areas including its use as a micro-radiosurgical tool to target specific tissue regions of biological samples,[10-15] as is the case for heavy-ion radiotherapy. Heavy-ion microbeams can inactivate specific cell populations in multicellular organisms by targeted irradiation and allow for the investigation of their function by observing changes in the irradiated targets. Similar analyses can be performed using micro laser ablation techniques. However, micro laser irradiation completely eliminates target cell and tissue structures as a result of heat-induced degeneration, while we can suppress cell division and gene expression without destroying intact tissue structures and intercellular interaction by heavy-ion microbeam irradiation. Moreover, the heavy-ion energy deposited at the Bragg peak can be controlled by adjusting the ion energy. Thus, heavy-ion microbeam irradiation can be employed in precisely controlled microsurgical operations with fewer side effects compared with micro laser ablation techniques.

Heavy-ion microbeam cell targeting system at JAEA-Takasaki

The heavy-ion microbeam system at JAEA-Takasaki employs a micrometer-sized collimator (microaperture) for

generating heavy-ion microbeams from ions accelerated using the azimuthally-varying-field (AVF) cyclotron.[16–18] This system has been used by JAEA-Takasaki group to irradiate a variety of samples including cultured cells,[16,19–21] nematode,[10] plant tissue[11,15] and silkworm.[12–14] The apparatus can generate microbeams with most of the ion species accelerated by the AVF cyclotron using various microaperture sizes ranging from 5 to 250 μm in diameter. The ion species frequently used include carbon (18.3 MeV/u), neon (17.5 MeV/u) and argon (11.5 MeV/u). For the irradiation of biological samples, ions are extracted into air from vacuum via a 8 μm-thick polyimide window or, in case of beam sizes less than 20 μm, extracted directly into air by maintaining the vacuum of the beam line through differential pumping. Irradiated ions penetrate cell samples cultured on the plastic ion track detector CR-39 (TNF-1, 100 μm thick), and are then detected and counted by the PMT-scintillator assembly installed on the revolver of the optical microscope used for cell irradiation. The system is designed for the rapid and simultaneous detection of ion hits on cell samples by visualizing the track on the counter side of CR-39 base plate as etched pits using an alkaline-ethanol solution under cell culture conditions (37°C, 5% CO_2 and 100% humidity). The variable beam size implemented by the exchangeable microaperture enables the system for use with a variety of biological targets from cultured cells in the micrometer-scale to silkworm larva in the millimeter-scale. Cells are stained with the fluorescent vital staining dye CellTracker Orange to locate the targets, and the position of the cells is then determined by image processing to generate the coordinate database using the "offline" microscope system, which is located away from the beam line to facilitate rapid irradiation. Following this, samples are transferred onto the "online" microscope, and then rapidly and automatically irradiated according to the coordinates stored in the database generated at the "offline" system. Because the position of beam is fixed, irradiation of sample is carried out by systematically moving each sample by the sample stage to the position of the beam. Target samples have included not only the cultured cells for radiobiological study, but also the root tissues of the thale-cress *Arabidopsis thaliana*, embryos and larvae of the silkworm *Bombyx mori*, and the nematode *Caenorhabditis elegans*, to investigate biological phenomena pertaining to a diverse group of fields including developmental biology, neurobiology and plant physiology. Detailed experimental procedures are described previously.[18]

Another microbeam system we are working on is newly developed focused heavy-ion microbeam system.[22,23] The system is equipped with a magnetic quadrupole quadruplet lens system for higher spatial resolution and with an X, Y beam scanner for fast hitting of single ion to micron scaled samples like a biological cell. In vacuum, a microbeam generated by the system had spatial resolution of less than 1 μm. To irradiate this finer microbeam to the specific region of individual cells, a new cell targeting system was designed and installed under the beam extraction window. The system consists of Olympus IX81 full-automatic inverted microscope system, and the set of automatic stages for managing sample and microscope alignment. The system is settled on the mount frame that is rigidly fixed to the quadrupole quadruplet lens for avoiding influences of vibration.

Biological applications of heavy-ion microbeam

Studies of direct hit effects of heavy ions

Chinese hamster ovary (CHO) cells were targeted with ^{40}Ar ion microbeams of 5 μm in diameter (11.5 MeV/u, LET = 1260 keV/μm), and the precise position of ion hits was determined by merged images of the cells and ion-pits etched on a CR-39 plastic ion track detector, showing that nuclear hits, comprising a single ion, and cytoplasmic hits significantly suppressed cell growth.[16] In addition to mammalian cultured cell lines, other cell types have been irradiated under *in vitro* culture conditions. As a model system representing single plant cells, tobacco BY-2 protoplasts were targeted with ^{12}C ion microbeams 20 μm in diameter (18.3 MeV/u, LET = 121 keV/μm) to investigate the clonogenicity of targeted cells.[20] As a model system for the investigation of muscular dystrophy where microinjury of the plasma membrane occurs,[24] single fibers isolated under *in vitro* culture conditions from mouse skeletal muscle were irradiated with ^{20}Ne (12.8 MeV/u, LET = 375 keV/μm) and ^{40}Ar (11.5 MeV/u, LET = 1260 keV/μm) ion microbeams 20 μm in diameter, and ultrastructural changes were examined using electron microscopy. We observed irregular protrusions and invaginations in the plasma membrane, irregular disruption of microfilaments in the cytoplasm near the plasma membrane, and multiple autophagic vacuoles. These findings suggest that heavy-ion irradiation causes disruption of the cellular architecture, and the removal of which involves autophagy.[24]

Studies of the bystander effects

With less than 0.02% of confluent AG01522 fibroblasts targeted with ^{20}Ne (12.8 MeV/u, LET = 375 keV/μm) and ^{40}Ar (11.5 MeV/u, 1260 keV/μm) ion microbeams 5 μm in diameter, we found that gap junctional intercellular communication and reactive oxygen species mediate bystander-induced micronucleus formation.[19,21] Recently, with less than 0.01% of confluent AG01522 fibroblasts targeted with ^{12}C (18.3 MeV/u, LET = 103 keV/μm), ^{20}Ne (17.5 MeV/u, 294 keV/μm) or ^{20}Ne (13.0 MeV/u, 375 keV/μm) ion microbeams 20 μm in diameter, we showed that bystander effects manifested itself as inactivated clonogenic potential, a transient apoptotic response and delayed p53 phosphorylation,[25,26] and that gene expression profiles in bystander cells are substantially different from those in irradiated cells.[27] We have also shown bystander-induced suppression of cell proliferation in CHO cell cultures using ^{40}Ar ion microbeams 5 μm in diameter (11.5 MeV/u, LET = 1260 keV/

μm).[16] With the *in vivo* targeting of germline cells in the nematode using ^{12}C ion microbeams 20 μm in diameter (LET = 120 keV/μm), we observed little, if any, bystander effects in nonirradiated bystander tissues.[10]

Studies using radio-microsurgical techniques

An example of plant physiological research by our group concerned the investigation of root gravitropism in thale cress.[11] Primary root apical tissues targeted with ^{12}C ion microbeams 120 μm in diameter (18.3 MeV/u, LET = 110 keV/μm) significantly suppressed root elongation and curvature at the root tip. Irradiation of cells that would later form the lower part of the root cap following gravistimulation resulted in dramatic inhibition of root curvature, an effect not observed following irradiation of cells that would form the upper part of the root cap. Targeted exposure to narrower microbeams (40 μm in diameter) revealed that inhibition of curvature was most pronounced at the root tip, followed by cells in the lower part of the root cap. These findings suggest that the most sensitive sites related to root gravity comprise the root tip and columella cells, and that the root gravity signaling pathway traverses the lower part of the cap cells following perception.[11] Recently, we also analyzed the function of the root cap and elongation zone cells in root hydrotropism using our 180-μm-diameter microbeams of ^{12}C ions (LET = 135 keV/μm).[15] Targeted irradiation of the elongation zone, but not the columella cells, significantly inhibited the development of hydrotropic curvature. Laser ablation as another microsurgical approach revealed that columella cells are indispensable for hydrotropism. Thus we showed that both the root cap elongation zone play indispensable and functionally distinct roles in root hydrotropism.[15]

To apply microbeam technology in the area of insect developmental biology, we investigated embryogenesis in the silkworm.[12] To this end, various sites within the eggs were exposed to ^{12}C ion microbeams (LET = 110–200 keV/μm) collimated using microapertures of varying diameter ranging from 60 to 250 μm. Targeted irradiation resulted in the generation of abnormal embryos which exhibited localized defects of organs including deletion, duplication and fusion in a manner dependent on the dose, beam size and choice of target site. Taking into account the close correlation between the location and frequency of these phenotypic defects on the resulting embryos and the targeted sites, we succeeded in establishing a fate map for the cellular blastodermal stage embryo.[12] The knob-forming region in first instar larvae of the knob mutant silkworm, which exhibit knobs on the dorsal side of larva spots, were also targeted with ^{12}C microbeams 180 μm in diameter (LET = 128 keV/μm), and knob formation was found to be suppressed at the irradiated segments.[14]

To evaluate the radiation effect on individual organisms, we investigated positional radiation effects on nematode germline cells.[10] In this study, germline cells in the gonad were irradiated with ^{12}C ion microbeams 20 μm in diameter (LET = 120 keV/μm). Targeted irradiation of the tip region of the gonad arm at the L4 larval stage arrested germ cell proliferation, while irradiation of the pachytene region at the young gravid stage induced apoptotic cell death in the gonad. This was also observed in the *c-abl-1* mutant nematode.[10] Thus, radio-microsurgical approaches employing targeted irradiation with heavy-ion microbeams generated at JAEA-Takasaki proved to be useful in characterizing the tissue-specific, local biological response in eukaryotes.

SINGLE PARTICLE IRRADIATION SYSTEM TO CELLS: SPICE, AT NIRS

Outline of the single particle irradiation system to cells: SPICE

An electrostatic accelerator facility of NIRS supplies protons and helium ion beam with a Tandetron accelerator (High Voltage Engineering Europa B.V.) at maximum energies of 3.4 MeV and 5.1 MeV, respectively. In this PIXE Analysis system and Tandem Accelerator (PASTA) facility, there are four beam lines,[28] and its three horizontal beam lines, conventional (*in vacuo*), in air and droplet[29], and microbeam scanning beam line[30] are available for PIXE analysis. In the fourth beam line, a single particle irradiation system to cells, SPICE has been constructed.[31,32] The beam is transported upward with a 90 degrees bending magnet installed in the middle of the microbeam scanning PIXE beam line. In order to get a microbeam in SPICE, the beam is focused by a mono bloc triplet lens so as to exclude low-energy, scattered particle components as often seen in other microbeam facilities utilizing collimation methods.

Beam size measurements using CR-39

The beam size was determined by irradiating a plastic track detector, CR-39. A CR-39 (100 μm thick) was adhered to the cell dish instead of cells, and then the dish was set on the voice coil motor-driven sample stage. The gap between the beam exit window, Si_3N_4 membrane (1 μm thick), and the targeted CR-39 was approximately 300 μm. Then, CR-39 was etched in 7M NaOH at 70°C for 2 hours and its image was obtained by confocal laser microscope (FV1000, Olympus). Figure 1 shows an image of irradiated CR-39 after the etching procedure. For each position, protons were irradiated by moving the sample stage with 50 μm pitch. Irradiation was performed automatically according to a text file containing data on a preset number of protons and on the X-Y coordinates of the sample stage position. This system enables one to irradiate 6–8 positions per second.

Cell targeting and irradiation system

For the routine irradiation on cells, the beam intensity is controlled to be below 5.0×10^4 protons per second. The number of protons having traveled through the cells is counted using a scintillation detector equipped on a microscope

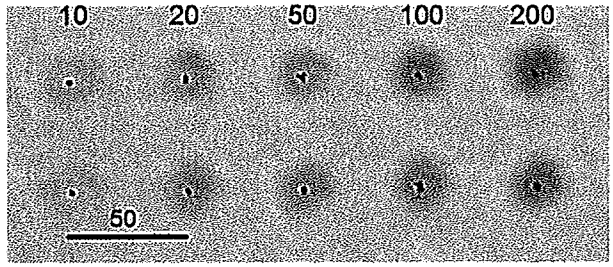

Fig. 1. Image of irradiated CR-39 after the etching procedure. 10 different positions on CR-39 were aimed at by moving the sample stage with 50 μm pitch. Number of protons irradiated for each position are indicated in the figure. Bar size, 50 μm.

system, which was set above the cell dish. Configuration of the components around the beam exit, such as the microscope, voice coil motor-driven sample stage, scintillation detector, and cell dish, are shown in Fig. 2. The system controlling PC controls a voice coil motor-driven sample stage, which was developed with Techno-hands, Co., Ltd., and also controls a fast beam deflector (10 MHz), which was installed upstream of the 90-degree bending magnet, with high-speed trigger pulse to turn on/off the beam. It is possible to irradiate with precise number of protons from one to an arbitrary number per position or cell. The nuclei of the cells are dyed with Hoechst 33258, and fluorescent images were captured by a 20× objective lens and a CCD camera (ORCA-ER, Hamamatsu) equipped on the microscope (BX51, Olympus). The size of single image frame was 430 μm × 330 μm, and the fluorescence of dyed cell nuclei within 3 mm × 3 mm area can be captured by taking 7 × 9 images. From these images, the X-Y coordinates of the cell position according to the fluorescence are calculated. An example of fluorescence image of nuclei of CHO-K1 cells dyed with Hoechst 33258 is shown in Fig. 3. The surrounding ellipse of each cell nucleus was drawn using self-developed cell recognition algorism based on a least-squares technique.[33] Each nucleus was numbered to identify the cells for irradiation experiments afterward. All of the irradiation procedures can be performed automatically after setting some parameters, such as a preset number of protons.

Cell dish and sample preparation

The cell dish was designed to culture a larger number of cells in a single dish and to reduce the air gap between the cells attached on the bottom of dish and the beam exit window. The air gap is adjusted to be below 300 micrometers to reduce beam scattering by the air gap. Photograph of cell dish is shown in Fig. 2B. Dish for the system was designed so as to sandwiching 2.5 μm thick Mylar film between a 30 mm diameter steel ring and a 33 mm diameter hole. Cells can be cultured on a area of 30 mm in diameter. On the surface opposite to the cell, blue lines are drawn with a permanent marker to define the origin of coordinates in the cell dish. This origin is used for describing the X-Y coordinates of the cells in the dish in imaging process for cell targeting and cell observation. Cells are seeded in this dish at 37°C under 5% CO_2 for 5 hr before irradiation, and stained with 1 μM Hoechst 33258 1 to 2 hrs prior to irradiation. Just before irradiation, the media were replaced with 1 ml of phosphate buffered saline (PBS). After 6 μm thick polypropylene (PP) film was floated on the surface of the PBS, PBS was removed, so that the cells were covered with PP film to avoid them from drying. Cell dish thus prepared is placed on the sample stage for irradiation.

Preliminary cell irradiation experiment

In order to confirm the performance of the system, reactive oxygen species, ROS, produced in the cell irradiated with microbeam were detected. ROS are important for understanding the effects of radiation-induced cellular damage. Many fluorescent probes have been developed for this purpose.[34] Among them, 2,7-dichlorofluorescin diacetate (DCFH-DA), has been used frequently in radiation biology for quantifying oxidative events in cells. DCFH-DA is absorbed by cells, and is rapidly deacetylated by intracellular esterases to 2,7-dichlorofluorescin (DCFH); subsequent oxidation of DCFH produces the fluorescent product 2,7-dichlorofluorescein (DCF).[35] We applied this method to

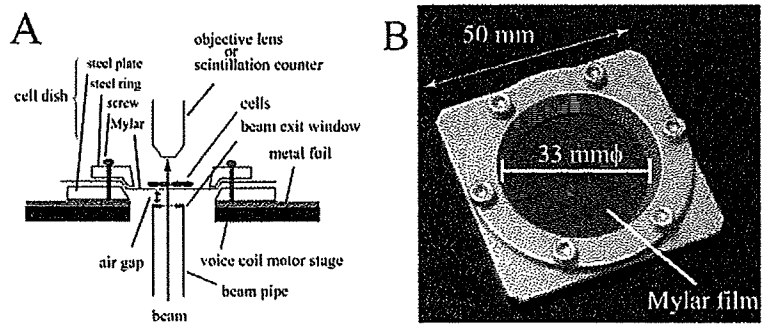

Fig. 2. Panel A is a drawing of the setup around the beam exit. Panel B is a photograph of the cell dish.

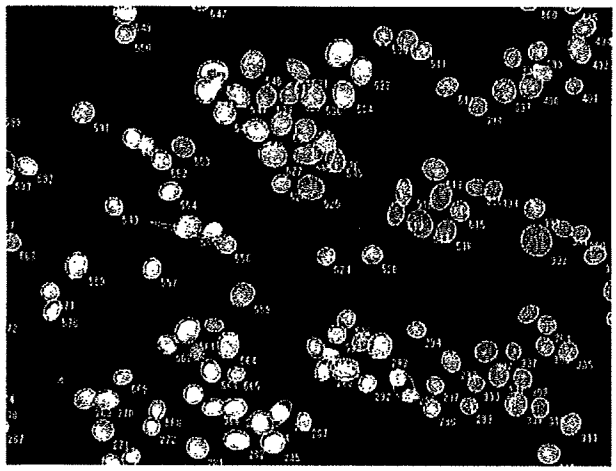

Fig. 3. Example of the fluorescent image of the cell nuclei obtained with the microscope system. The surrounding ellipse of each cell nucleus represents the results of automated cell recognition, and the identification numbers and X-Y coordinate are computed automatically.

detect ROS induced intracellularly with 3.4 MeV proton microbeam.

CHO-K1 cells were cultured in α-MEM containing 10% fetal bovine serum with appropriate antibodies. To detect the 3.4 MeV proton-induced of ROS with DCFH-DA probes, cells were seeded in a microbeam dish 24 hr prior to irradiation. Approximately 80% of cells were confluent at the time of irradiation. Approximately 2 hrs prior to irradiation, the medium was changed to medium containing 1 μM Hoechst 33258, and 30 minutes prior to irradiation, the medium was replaced with DCFH-DA solution (100 μM DCFH-DA in PBS). The targeting procedures were completed in less than 5 minutes after placing the cell dish onto the sample stage. Targeted cells were selected manually on the fluorescence image of dyed cells. Figure 4A shows the fluorescent image obtained by the microscope, and a) ~ d) are the four cell nuclei targeted. The preset numbers of protons for the targeted cell nuclei, a)–d) were 5×10^4, 1×10^5, 2×10^5, 5×10^5, respectively. Figure 4B shows the fluorescent product DCF, which was the result of ROS production by the proton traversal through the cell nuclei. The intensity of fluorescence in those irradiated cells was shown to increase with increasing number of protons irradiated. Further investigation is under way concerning the detection of induced DNA damage, cell cycle arrests, and cell inactivation with irradiation of below one hundred protons.

Summary and future work

We have developed the microbeam irradiation system, SPICE. Approximately 5 μm beam in diameter is available now, and irradiation with single proton can be performed. The maximum speed for cell irradiation is 400–500 cells per minute with aid of automated imaging sysytem, and most of the irradiation procedures can be performed automatically by setting some parameters. As a demonstration, CHO-K1 cells were irradiated and the production of reactive oxygen species ROS in the targeted cells was detected. Further improvements are on the way, such as an off-line microscopic system for post-irradiation biological analysis, improvements on targeting accuracy and its beam size below 2 μm in diameter. SPICE and PASTA are now an open facility for collaborative researches.

SINGLE CELL IRRADIATION SYSTEM AT THE WAKASA WAN ENERGY RESEARCH CENTER

Introduction

Recently, the application of microirradiation techniques in biology has attracted much interest, as such techniques make it possible to irradiate individual cells with ions under precise dose control, thus providing a unique opportunity to study the inter- and intracellular responses of individual cells to low-dose irradiation. A number of microirradiation systems for radiobiology have been developed and are now

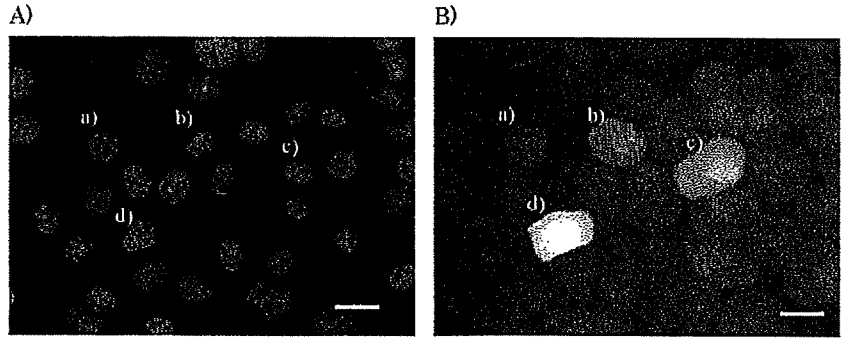

Fig. 4. Panel A shows the fluorescent nuclei image Targeted nuclei are indicated as a)–d) in Panel A, which were irradiated with 5×10^4, 1×10^5, 2×10^5, 5×10^5 protons, respectively. Panel B shows the fluorescent product, DCF, which was the result of ROS production by proton traversal through the cell nuclei.

operational.[1,2,36,37] A single-cell irradiation system is currently under development at the Wakasa-wan Multi-purpose Accelerator with Synchrotron and Tandem (W-MAST).[38] Cells are irradiated using a vertical ion beam, with collimation achieved using a glass capillary.[39] This report presents the design and construction of this single-cell irradiation system, and provides some results demonstrating the capabilities of the system.

Experimental facility

Beam line

The beam line for cell irradiation is installed in Irradiation Room 2 at the W-MAST facility. A proton or helium beam accelerated by the tandem accelerator is used for single-cell irradiation. The linear energy transfer (LET) in the water and range are 4.7 keV/μm and 1.2 mm for the 10 MeV proton, and 41 keV/μm and 215 μm for the 15 MeV helium ion, respectively. Figure 5 shows a side view of the beam line. The beam, transported vertically, is collimated with two apertures of 2 mm and 0.5 mm diameters. The distance between two apertures is 346.5 mm. After rough collimation, beams are extracted in air through a glass capillary with a 5 or 10 μm inner diameter. The angular spread of the ion beam due to the geometry of the collimators is estimated to be 1 mrad. Tilt and position of the glass capillary are adjustable, and the glass capillary is aligned so that the energy spread of the collimated beam is minimized. After collimation, the beam is extracted into air through a Mylar foil and irradiated to the cell.

Stage and microscope

The stage for cell irradiation is installed immediately below the beam exit. The stage is driven by motors and can move in the *x*, *y*, and *z* directions. A size of the sample stage is 246 mm × 246 mm, and dishes of 60ϕ or 35ϕ, or chamber slides can be settled on the stage. Cells are cultured on a CR39 sheet, which is pasted on the bottom of a perforated dish. When the cells are irradiated, they are covered with a polyimide foil for the prevention of dehydration. An optical microscope with a charge coupled device (CCD) camera is mounted beneath the irradiation stage to obtain images of living cells. A silicon surface detector (SSD) is also mounted in one of the ports on the objective-lens revolver of the microscope. The SSD is covered with an Al foil of 2 μm thickness for the light shield. The SSD is utilized for the measurement of the energy spectrum of the collimated beam and for the ion counting. Images of cells are processed and viewed on a PC, and the positions of individual cells are calculated in stage coordinates. The determination of the beam position is performed by observing beam fluorescence of a plastic scintillator placed at the target position. Before the irradiation, we observe cells with the microscope, move them to the beam position and record coordinates on the stage. At the irradiation, the number of incident ions is counted with the SSD.

Single event control

The number of ions incident at the cell is controlled by electrostatic deflection of the ions together with ion detection using a silicon surface-barrier detector (SSD). Figure 6 shows a schematic diagram of the control system. The electrostatic deflector, which is used for the beam blanking, is installed on the injection line into the accelerator. When the cell is irradiated, the number of ions which have penetrated through the cell is counted using the SSD. When the number of signals reaches a preset number, the output signal from the preset scaler activates the high-voltage unit driving the electrostatic deflector. For single-event control, it is necessary to irradiate cells at a rate of less than 100 ions/s due to the relatively slow response (~1 ms) of the high-voltage unit.

Sequential irradiation control

Individual cells at different positions on the stage can be irradiated sequentially using the automatic control system shown schematically in Fig. 6. Automatic control is performed via a PC equipped with 4 peripheral boards providing digital I/O (DIO), counter, serial interface and video capture functions. The motor controllers for the stage movement and the image-processing unit for the optical micro-

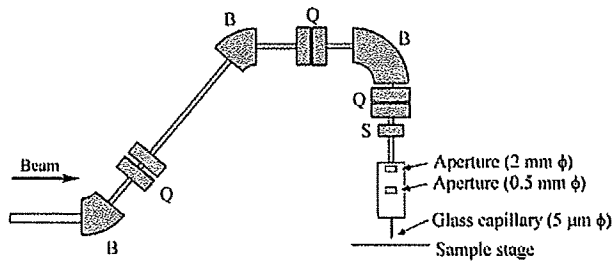

Fig. 5. Side view of the single cell irradiation beam line. B, Q, S denote bending, quadruple and steering magnets.

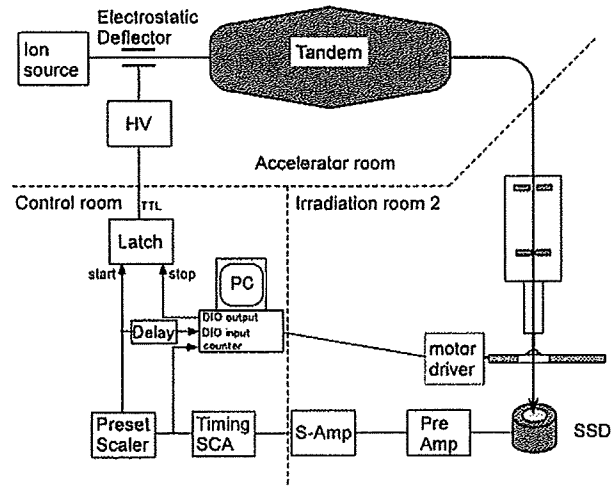

Fig. 6. Schematic diagram of the single-cell irradiation system.

scope are connected to the PC via an RS-232C interface. The DIO board is connected to a NIM module that generates a control signal for the high-voltage unit driving the electrostatic deflector. Before irradiation, the position data for individual cells are input into the automatic control software. Irradiation is started after positioning of the stage. When the number of ions detected with the SSD reaches a preset number, the output signal from the preset scaler is received by the DIO board to activate the high-voltage module for the electric deflector. Then the motor controller moves the stage under automatic control to the next irradiation position. After the movement is complete, the DIO board outputs a signal to deactivate the electrostatic deflector and thereby start irradiation on the next cell. The number of protons for each cell position is recorded in the PC.

Results of experimental tests

At first, energy spectrum of the collimated beam was measured using the SSD. The helium beam with energy of 15 MeV was extracted into air through a Mylar foil of 2 μm in thickness. The glass capillary of 5 μm inner diameter was used for the measurement. The SSD was positioned in air 15 mm below the exit window. The measured energy spectrum shows that 93% of the detected helium ions are distributed near the high-energy end, forming a peak in the spectrum. In the case of the proton beam with energy of 10 MeV, 78% of the detected protons are in the peak at the high-energy end using the glass capillary of 10 μm inner diameter.

The beam sizes were measured using CR-39 track detectors placed about 1 mm and 2 mm below the beam exit window when 15-MeV helium beam was extracted through the capillary of 5 μm inner diameter. After etched in 6 N NaOH at 60°C, the track distribution observed under a laser microscope (Fig. 7) shows that the beam spread was about 10 μm on the CR-39 placed 1 mm below the beam exit window. When placed 2 mm below of the beam exit, the beam spread was about 20 μm. The beam sizes thus estimated were larger than the inner diameter of the capillary (5 μm). The angular spread of protons due to multiple scattering in the beam path, especially at the beam exit window, is considered to be responsible for this beam broadening.

Figure 8 shows the incidence pattern obtained by automatic irradiation of the CR-39 track detector to draw the letters 'WERC'. The letters were about 100 μm tall each, and consisted of total 76 points, with 50 counts per point. The letters 'WERC' can be recognized clearly, which shows that the automatic irradiation is performed successfully. Tracks distributed randomly around the letters are presumably due to edge scattering at the capillary.

Summary

A system for irradiating single cells with controlled ion doses has been developed at the W-MAST facility. The collimated ion beam delivered vertically is used for the irradiation. The system is controlled using a PC and NIM modules to allow sequential cell irradiation. The results of test experiments revealed that 93% of the collimated helium ions were mono-energetic and that the beam spot was about 10 μm. Automated irradiation of a CR-39 track detector demonstrated the sequential irradiation successfully. Further developments for the determination of the beam position at the target position and for observing living cells with the microscope are needed for the single cell irradiation.

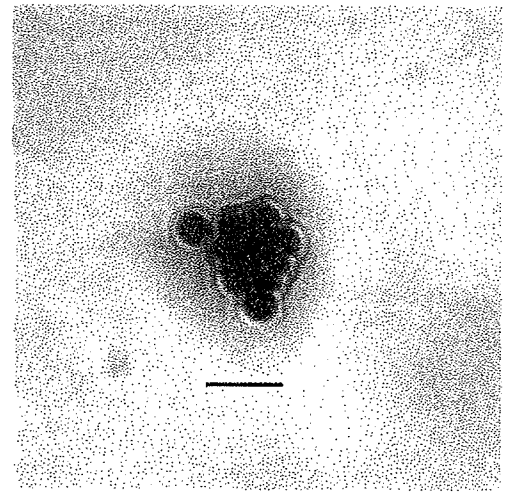

Fig. 7. Beam size measured using a CR-39 track detector. Bar is a 10 μm-long scale.

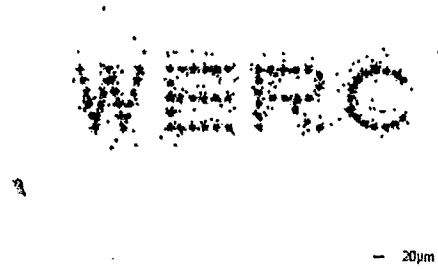

Fig. 8. Incidence pattern after automated irradiation of the letters 'WERC'. Each letter is about 100 μm tall.

NAGASAKI UNIVERSITY SOFT X-RAY MICROPROBE

Composition of the system

There are a couple of microbeam facilities in the world including those settled in Nagasaki University. Nagasaki University had conducted so called the 21st century Center Of Excellence (COE) program between 2002 and 2007. The title of the program was "International Consortium for Medical Care of Hibakusya and Radiation Life Science", and, in

order to promote researches toward low dose radiation effects, Nagasaki University COE program introduced Soft X-ray microprobe, which was originally developed in Gray Cancer Institute in United Kingdom.[40] The Nagasaki University soft X-ray microprobe consists of three major parts, which are the microfocus X-ray source, the X-ray focusing assembly, and the cell imaging and alignment unit. Focused electron bombardment of a carbon target generates characteristic X-rays (278 eV). A continuum of bremsstrahlung is removed by reflecting the radiation off with a 25-mm-diameter silica mirror placed between the target and the X-ray focusing assembly. Focused X-rays are obtained using zone plate, which is made from tungsten deposited on a 100-nm-thick silicon nitride substrate, together with the order selecting aperture (OSA). Cells are cultured on a 0.9-μm-thick mylar membrane, firmly placed at the bottom of metal dish, which is clamped to a two-axis, stepped-motorized microscope stage. They are stained with the DNA-binding dye Hoechst 33258, and the nuclear image is captured by an intensified charge-coupled device. Then, the experimenter selects a cell or cells to be targeted using an on-screen computer mouse pointer. As reported previously, dose distribution to the cell is not homogeneous. For example, about 40% of the dose is deposited in the first micrometer of the cell. About 50% of the dose is absorbed in the lower half of the nucleus, while 6% is absorbed in the upper half. Based upon the absorbed energy in the nucleus divided by the nuclear mass, a Chinese hamster V79 cell would receive 1 Gy with about 10,000 photons.

Localized Photon Delivery System (LPDS)

Recent studies using soft X-ray and alpha-particle microbeam irradiation further extended our knowledge of radiation effects.[41,42] However, the application of micro-irradiation technique is not only limited to the studies in the field of radiation biology. As microbeam is capable of depositing radiation energy to a very limited area within a cell, *micro irradiation*, we now call this system as localized photon delivery system (LPDS), provides unique opportunity to investigate physiological functions of micro-components of the cell constituents. For example, while DNA has been treated as a primary target for radiation exposure, there are increasing numbers of literature reporting a role of protein damage on radiation effects.[43–45] It is likely that ionized proteins reveal altered functions. In fact, long-lived protein radicals are supposed to be involved in radiation-induced mutagenesis.[43] Because LPDS deposits radiation energy only to the nucleoplasm or cytoplasm, it can separate radiation effects stem from DNA damage and protein damage. It was also shown that extremely low-dose radiation stimulates growth factor receptors, which result in activation of mitogen-activated protein kinase pathway.[44] LPDS is able to deposit dose only to the membranes. Thus, LPDS is highly expected to be applied to the experiments investigating such non-DNA effects. Moreover, advanced technology using fluorescence protein-tagged proteins enables visualization of target proteins in a living cell. For example, an expression of EGFP-tagged tubulin illustrates spindle fibers, whose dysfunction causes mitotic defects. Microirradiation to a part of spindle fibers may lead to miss-segregation of the chromosomes. Furthermore, as a pioneer study lead by Cremer has proven its possibility,[46] LPDS could be a clue to depict higher-order chromatin organization in the cell nucleus. Since the width of the finest microbeam is expected to be sub-micrometer, which corresponds to the size of several megabase-chromatin domains, it is possible to examine the effects of disorganization of chromatin domains on a stability of chromatin territory, chromatin movement, and on interaction of damaged chromatins. Although previous studies have applied UV laser for such purpose, future studies of chromatin dynamics cannot be accomplished without PLDS.

Biological results and future perspectives

Our group has been applied LPDS for investigating DNA damage response in mammalian cells. As reported previously, radiation-induced DNA double strand breaks initiate activation of DNA damage checkpoint pathway. DNA damage-induced higher-order chromatin disorganization dissociates ATM dimers or oligomers to the monomers, whose process is essential for the execution of DNA damage response. Activated ATM through autophosphorylation at serine 1981 phosphorylates downstream effectors, such as histone H2AX, 53BP1, MDC1, NBS1, and p53. It has been shown that these phosphorylated effectors as well as phosphorylated ATM form discrete foci, which are detectable as dotted signals by immunofluorescence analysis. Foci of each factor are always co-localized, indicating that foci formation is phosphorylated ATM-dependent. Because the number of foci is equivalent to that of DNA double strand breaks, it is generally believed that the foci visualize chromatin regions that have DNA double strand breaks. We have reported the dose-dependent induction of phosphorylated ATM foci, and more recently, we successfully visualize phosphorylated ATM- and phosphorylated histone H2AX-dependent formation of 53BP1 foci in situ, by introducing the EGFP-tagged 53BP1 gene into normal human diploid cells. Our current study illustrates dynamic process of 53BP1 foci formation, whose dynamics is tightly related to the cell cycle checkpoint regulation. Such studies using live cell imaging technology must be the future trend to understand the dynamics of cellular response to radiation.

Summary

Nagasaki University soft X-ray microprobe has now offered a unique opportunity to study the mechanism of non-targeted effects of ionizing radiation. There is also considerable interest in the application of LPDS for a wide variety

of research fields. Our collaborative works are expected to contribute to the better understandings of the radiation effects on living organisms.

THE CRIEPI MICROBEAM SOFT X-RAY IRRADIATION SYSTEM

Introduction

Today, many facilities have been developed and planned microbeam irradiation systems using charged particle radiations (see in extended abstracts of 8th International Workshop: Microbeam probes of Cellular Radiation Response). However, X-ray microprobes, which have been developed and operated constantly, were only at the Gray Cancer Institute (UK)[40,47] and at the Photon Factory utilizing SR X-rays.[37,48] Microbeam soft X-ray irradiation system at Central Research Institute of Electric Power Industry (CRIEPI), Tokyo, Japan, has been developed in March, 2007 to investigate cellular response to low dose radiation and non-targeted effects, such as radiation-induced bystander responses, adaptive responses and genomic instability. Our system is characterized by (1) tabletop (2) X-ray focusing system using Fresnel zone plate (FZP), and (3) on-line confocal laser microscope.

The X-ray source and the focusing assembly

Following the Gray Cancer Institute ultrasoft X-ray microprobe,[40,47] Fresnel zone plate (FZP) is used to focus characteristic X-ray generated by the electron bombardment of a target. The electron gun is OME-0055LBW (Omegatron) with lanthanum hexaboride (LaB_6) cathode, which can generate a high-brightness focused electron beam, and is operated at voltages up to –30 kV relative to the target (Fig. 9C). The electron beam is focused with electromagnetic lens onto the surface of the target made of aluminum. Rotary pumps, turbo molecular pumps and vacuum gauges are set to the electron gun chamber and the target chamber independently. The electron gun is connected with the target chamber with a gate valve. To keep the LaB_6 filament in a good condition, pressure in the electron gun chamber and the target chamber is always kept at 10^{-7}–10^{-8} Torr.

Characteristic K-shell X-ray of aluminum (1.49 keV) is generated by the focused electron bombardment of an aluminum target (Fig. 9D). Hereafter, "soft X-rays" will be used to denote 1.49 keV X-rays. The bremsstrahlung X-rays having higher energy, which are also generated together with characteristic radiation, are removed by reflecting the grazing incidence mirror. This mirror is 20 mm × 10 mm made of Au (Fig. 9E). The incident angle is 1.5°. The vacuum window is made of 0.3 mm × 0.3 mm silicon nitride, which is 150 nm thick (Fig. 9F). The FZP is 150 μm in diameter, designed and manufactured by NTT-AT Nanofabrication (Fig. 9G). Exposure period is controlled using the shutter (Fig. 9H). The order selecting aperture (OSA) is used to select first-order diffracted soft X-ray by blocking unwanted zero and higher-order X-rays. The OSA consists of the pinhole, 30 μm in diameter (Fig. 9I). From the vacuum window to the OSA, helium gas is continuously blown to minimize attenuation of the soft X-ray.

The Cell imaging and irradiation

Autostage, cell irradiation dish and irradiation software are same as the synchrotron X-ray microbeam irradiation system at the Photon Factory (PF), High Energy Accelerator Research Organization (KEK, Ibaraki, Japan).[37,48] Cells are plated on the 1.5 μm-thick Mylar film based cell irradiation dishes (34 mm in diameter, Fig. 10A).[37] We have developed custom-made stage top incubator (Tokai Hit, Shizuoka, Japan) that accommodate cell irradiation dish to enable real-time live cell analysis (Fig. 10B).

High resolution cooled CCD camera (ORCA-ER, Hamamatsu Photonics) is combined with irradiation system. To irradiate cells, the beam position is detected using a scintillator and records the coordinates of the center of soft X-ray microbeam. Cell nuclei are stained with Hoechst 33258 at a concentration of 1 μM for 30 min before irradiation. After twice wash with PBS, cells are incubated in a fresh medium for the irradiation. The positions of cell nuclei are determined by the fluorescent image obtained using the CCD camera. The position of targets and exposure period are memorized in the irradiation software. For immunofluorescent study, confocal laser scanning microscope (FV300, Olympus, Tokyo, Japan) is also combined with irradiation system.

Characteristics of soft X-ray microbeam

The measurement of energy spectrum indicated that focused 1.49 keV of Al-Kα X-ray can be acquired at the sample position through the OSA (data not shown). Beam size was measured by knife-edge scanning and observed beam size was 1.8 μm in diameter (Fig. 11). Dose rate in the irradiated region was about 1 Gy/s under the usual operating condition.

Detection of DNA damage induced by soft X-ray microbeam irradiation

The induction of complex clustered DNA damage, having multiple DNA lesions within a few helical turns, has been considered as the cause of efficient cell killing of high LET charged particle radiations. To examine a possibility of the induction of complex clustered DNA damage induced by high dose of focused soft X-ray microbeam irradiation, human cervical carcinoma HeLa cells were irradiated with X-ray microbeam for 30 or 60 sec (about 30 or 60 Gy within irradiated region). Cells were fixed with cold methanol and rinsed with cold acetone 0.5 or 8 h after irradiation. DNA lesions induced by soft X-ray microbeam were visualized by immunofluorescence staining with anti-rabbit 53BP1 and

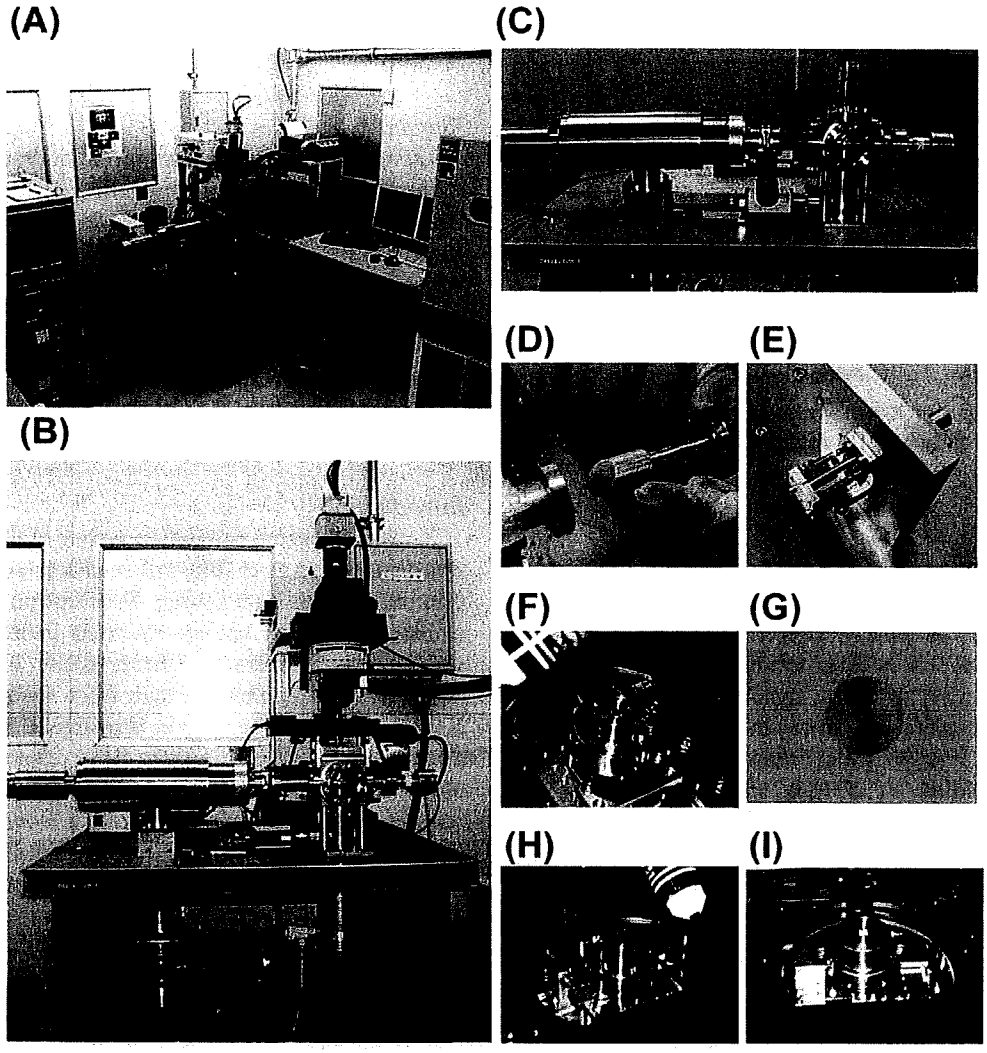

Fig. 9. Microbeam X-ray irradiation system of CRIEPI. (A) External view of system. (B) The X-ray microfocus source and confocal laser scanning microscope. (C) Electron gun and target chamber. (D) Aluminum target. (E) The grazing incidence mirror. (F) The vacuum window. (G) Fresnel zone plate (FZP). (H) The FZP assembly and the shutter. (I) Order selecting aperture (OSA).

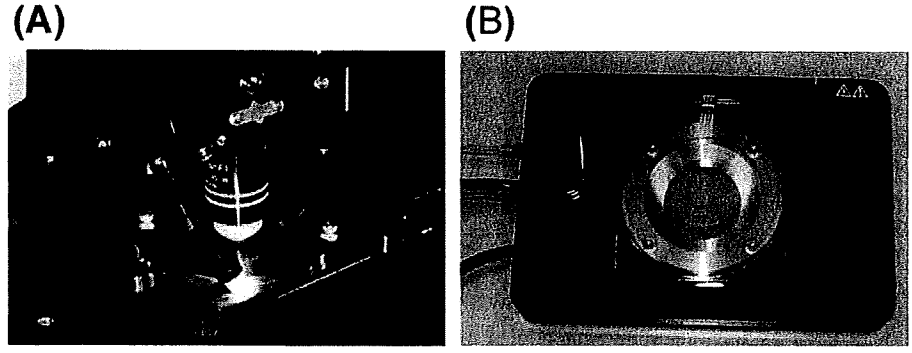

Fig. 10. Cell irradiation dish. The cell irradiation dish used in this system is same as that in synchrotron X-ray microbeam irradiation system, Photon Factory, KEK (Ibaraki, Japan). (A) Cell irradiation dish was set on autostage. (B) The stage incubation chamber.

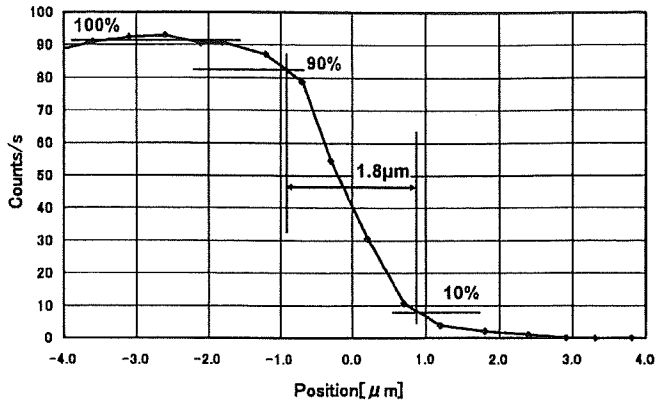

Fig. 11. The output of X-ray was measured by the scanning of photodiode set on autostage. Beam size could be estimated at 1.8 μm in diameter.

anti-mouse phosphorylated histone H2AX (Ser139, generally known as γ-H2AX) antibodies. Co-localization of 53BP1 and γ-H2AX could be clearly observed in the soft X-ray irradiated cell nuclei 0.5 h after irradiation (Fig. 12, upper panels). Localization of DNA repair proteins was disappeared within 8 h (data not shown) in cells irradiated with a few Gy of high energy, wide beam X-rays. On the other hand, co-localization of 53BP1 and γ-H2AX was not resolved even 8 h after high dose of X-ray microbeam irradiation and was not diffused from irradiated area(Fig. 12, lower panels), suggesting locally multiple-damaged site, or clustered DNA damage, may be induced with soft X-ray microbeam similarly as with high-LET charged particle irradiation.

Summary

Table-top microbeam X-ray irradiation system using Al_K X-ray has been developed at the CRIEPI, Tokyo, Japan. Obtained beam size was 1.8 μm in diameter and dose rate in the irradiate region was about 1 Gy/s. This system is now working routinely, and open to outside researchers under collaborative research.

MONOCHROMATIC X-RAY MICROBEAM IRRADIATION FACILITY AT THE PHOTON FACTORY

Introduction

X-ray microbeam irradiation system at the Photon Factory was designed so as to fully utilize characteristics of synchrotron radiation as light source. Synchrotron radiation (SR) is emitted from high energy electrons generated in electron storage-type accelerator. Characteristic of SR are strong intensity in wide energy range from vacuum-ultraviolet to X-rays, and nearly parallel or directional beam according to the relativistic effect. Using latter characteristics, X-ray microbeam can be produced either by simple cutting of beam with precise slit system or by a focusing system, such as Kirkpatrick Baez (K-B) mirror system. Both systems have merit and demerit; in former system, beam size can be

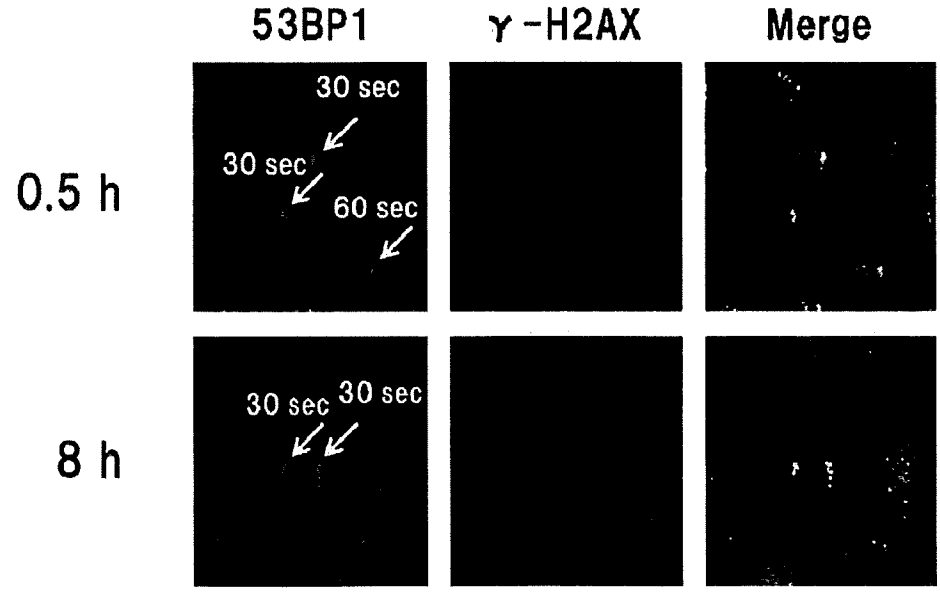

Fig. 12. Localization of 53BP1 and phosphorylated histone H2AX (γ-H2AX) was observed by immunofluorescence. HeLa cells were cultured on cell irradiation dish and irradiated with X-ray microbeam for 30 or 60 sec. Cells were fixed 0.5 h (upper panels) and 8 h (lower panels) after irradiation. Following immunofluorescence, cells were observed using online confocal laser scanning microscope.

changed arbitrarily above 5 μm square with constant intensity, in the latter, more intense beam (higher photon density) is available in smaller beam while change of beam size is not so easy. Considering these points, we decided to employ a precise slit system to obtain X-ray microbeam. We have developed three type of microbeam irradiation system. All the developed systems have been installed at BL-27B in the Photon Factory, Institute of Materials Structure Science, High Energy Accelerator Research Organization (KEK) in Tsukuba, Japan. Experimental stations at BL-27 are situated in the biological sample preparation area, where incubators and other equipments to grow and handle mammalian cells are available.

Energy-fixed (5.35 keV) X-ray microbeam irradiation apparatus

First type of the system is composed of three parts.[48] The first part is to produce X-ray microbeam by a high-precision slit system to cut out the beam. This slit system is set just below the sample stage. Minimum beam size obtained so far is 5 μm square by the slit system. Before making a microbeam, the beam is reflected right angle upward by diffraction of Si(311). Due to this process, energy of X-rays is fixed to 5.35 keV, which can penetrate into tissue nearly half mm deep. The second is an epi-fluorescent microscope equipped with a precise motorized stage, on which the sample dish is horizontally fixed and irradiated with X-ray microbeam. The third is a fluorescence image analyzer (computer) with a sensitive CCD camera, which recognizes the target cells and their positions. It also controls irradiation of X-ray beam to the targeted cells, one by one, automatically. Intensity of diffracted X-ray beam at the sample position is about 40 R/sec (ca. 10^4 photons/s in 10 μm square). Positioning accuracy of the targets, coordinates of which are automatically analyzed, are about 1 μm. This system can irradiate 1000 cells per hour, so that we can keep the cells in a good physiological condition during the irradiation process. Figure 13 demonstrates performance of our system. Distribution of immunostaining of γ-H2AX clearly depends upon the irradiated beamsize.

Energy-tunable X-ray microbeam irradiation apparatus

Second system developed is an energy-tunable X-ray microbeam system. One of the advantages of using SR as light source is that we can choose any energy of monochromatic X-rays with practical intensity. Using this merit we have a long experience in studying the energy dependence of X-ray-induced biological effects, including the effects of inner shell photoabsorption and Auger effects. According to the recent reports using microbeam, it has been revealed that radiation-induced signaling in the cell plays an important role for deciding the final biological effects. In order to study the signal induction process from energetic viewpoint, we

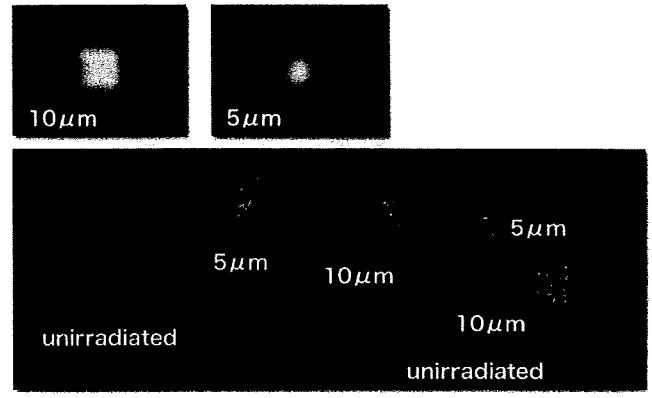

Fig. 13. Immunostaining (green) of γ-H2AX in cell nuclei (red) irradiated with microbeam of different sizes.

developed an energy-tunable X-ray microbeam system, by which we can irradiate with monochromatic X-ray of inner-shell absorption edges of certain elements. We have to use the horizontal beam as emitted from the electron storage ring, hence we need to overcome some difficulties such as vertical positioning and sample chamber containing cells. After confirming the accuracy/reproducibility of sample positioning stage within a few micron, we have studied the effects of microbeam X-ray tuned to the absorption edges of endogenous Ca and Fe which is incorporated as phenanthroline-Fe.

Irradiation apparatus aiming at cytoplasm

Third one was designed to irradiate cytoplasm only, avoiding irradiation to cell nuclei. Using the advantage of our slit system, we have measured dose-survival relationships of V79 cell in two irradiation conditions with clonogenic assay.[49] One is to irradiate with 10 μm square beam aiming at nucleus only, the other with 50 μm square aiming at whole cell. This work revealed that hypersensitivity in low dose region is more enhanced in nucleus-irradiated cells than in whole-cell irradiated cells. These results suggest that intracellular communication between nucleus and cytoplasm plays an important role in determining the cell death in low dose region. For further investigation of intracellular communication in irradiated cells, we have developed a system to irradiate cytoplasm only without irradiating cell nucleus. In order to shield the nucleus from irradiated in the uniform irradiation field, we made a gold mask, 15 μm in diameter and 20 μm thick, on a very thin (200 nm thick) SiN film. The thickness of the gold was determined to decrease the intensity of 5.35 keV X-rays to less than one-thousandth. SiN film is nearly transparent (more than 99% transmission) to this energy of X-rays. SEM image of this mask is shown in Fig. 14. The mask was mounted on a small X-Y stage and set in the X-ray path between the slit system and the sample stage. Using the scintillator dish to observe the shape and

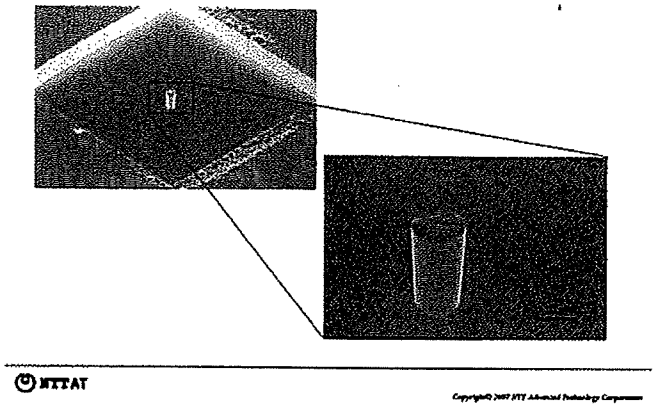

Fig. 14. SEM image of the mask. (provided by NTT-AT).

position of the X-ray beam, we adjusted the position of the mask and the size of the beam. Finally, we got a 50 μm by 50 μm beam with uniform intensity, at the center of which located was dark area of 15 μm diameter by the gold mask. Image of the beam taken as fluorescent intensity of scintillator is shown in Fig. 15.

When we want to irradiate only cytoplasm of the cells, center of the mask was recognized as the beam position and cytoplasm of cells, nuclei of which were stained with Hoechst dye and recognized by its fluorescence, were irradiated with X-rays, leaving nucleus unirradiated. Survival data are now being accumulated and survival curve of cytoplasm-irradiated cells will soon be presented.

Summary

Three types of X-ray microbeam irradiation apparatus have been developed and now working routinely using synchrotron X-rays at the Photon Factory, KEK, Tsukuba, Japan. Energy range available now is from 4 keV up to 20 keV. Beam size can be changed easily from 5 μm square or above.

DEVELOPMENT OF THE CAS- LIBB SINGLE-PARTICLE MICROBEAM

Introduction

The research team in the Key Laboratory of Ion Beam Bioengineering, Chinese Academy of Sciences (CAS-LIBB), in Hefei, China, proposed a Single Particle Microbeam (SPM) program for radio-biological irradiation in 1991, and put forward a further project of a SPM in 1995. In 2002, a high-quality SPM facility was installed. After two years of adjustment and optimization, the SPM facility has achieved perfect performance. Thereby, an ideal research platform is provided for studies on risk assessment on low-dose environmental exposures, genomic instability in cells, "bystander effects" and the underlying mechanisms of radiation damages in living cells, etc..[50]

Facility components and modules

The CAS-LIBB microbeam facility is comprised of these elements: 1) a 5.5-MV Van de Graaff accelerator, 2) two deflecting magnets for producing mono-energetic charged particles beam, 3) the beam-transporting pipeline with feedback devices, magnetic quadrupoles, diaphragms and vacuum bumps, and 4) electric beam shutter and the microbeam collimator at the end-station. Figure 16 shows the beam line layout of the facility. Ions produced from a radio-frequency (RF) ion source are accelerated to an energy in the range of 2.0–3.0 MeV and transported to the first beam-deflecting magnet through a beam guider and a pair of collimation slits. After the first deflection, the mono-energetic beam goes forward horizontally through the beam-stabilizer, quadrupole magnets and the beam shutter plates, and then enters the second beam-deflecting magnet. The up-going

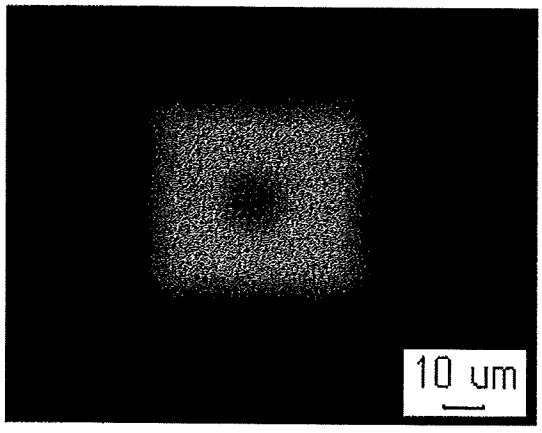

Fig. 15. Shape of the X-ray microbeam aiming at cytoplasm only.

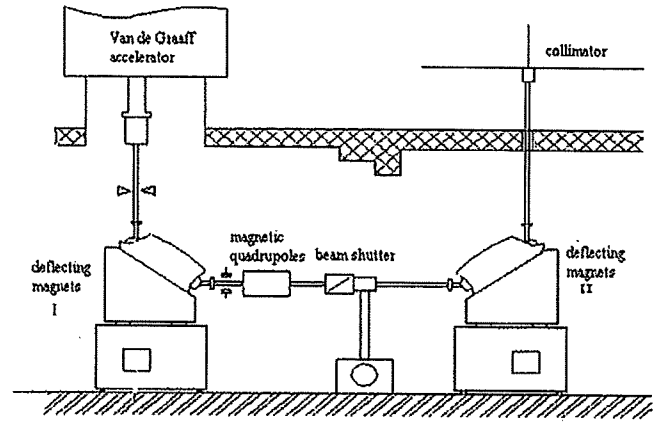

Fig. 16. Beam line layout of the single-particle microbeam facility.

beam deflected by the second magnet travels vertically through another collimation slits and finally enters the microbeam terminal room.[1,2,51–53)]

It should be possible for the SPM facility to irradiate a pre-selected target with the accuracy down to several microns or even less to realize fully its potential. Two successful methods are available for forming microbeam: collimation and focusing. For low-energy ion irradiation of sample cells grown outside vacuum, employment of a collimated microbeam is preferred owing to simplicities of the setup and its operation.[1,2,36,51,52,54–57)] Experimental results have demonstrated that a μm-diameter collimated microbeam has a sufficient resolution for cellular or sub-cellular irradiation.[58–60)]

We adopt the collimation method for the CAS-LIBB microbeam facility. A borosilicate glass capillary with 1-μm inner diameter, 210-μm outer diameter and 980-μm length is used as the collimator exit, which is mounted in the center of a holder at the end of the beam line. The verticality of the collimator is adjustable by fine adjustment screws. A multilayer film system had been used as the particle detection system successfully, as show in Fig. 17(A). Now, We have modified the structure of the particle detection system and studied the influence to the properties of single particle microbeam. Plastic scintillator wrapped by 7 μm Al foil was replaced by plastic scintillator which was deposited by 500 nm Ag film using magnetron sputtering. (Fig. 17(B)). Our results suggest that this modification can improve the space and energy resolution of CAS-LIBB SPM as well as the depth of incidence.

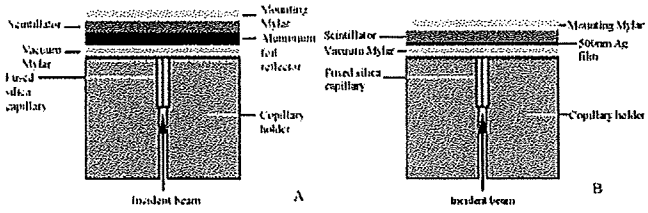

Fig. 17. Structure of the collimator and the scintillator. (A) Original design (B) New design.

Single-particle detection efficiency and cell location accuracy are two key indexes for the single-particle irradiation. Additionally, reliable monitoring and timely feedback of information from the key parts of the facility are also essential for a smooth operation. These performances require an efficient computer control over the whole components in the facility. The computer control program of the CAS-LIBB facility includes three logical modules: 1) the data acquisition and image processing for the sample cells, 2) the control of the auto-scanning sample stage, and 3) the single-particle detection and beam shutter controlling, as illustrated in Fig. 18.

The cell image recognition and processing are co-

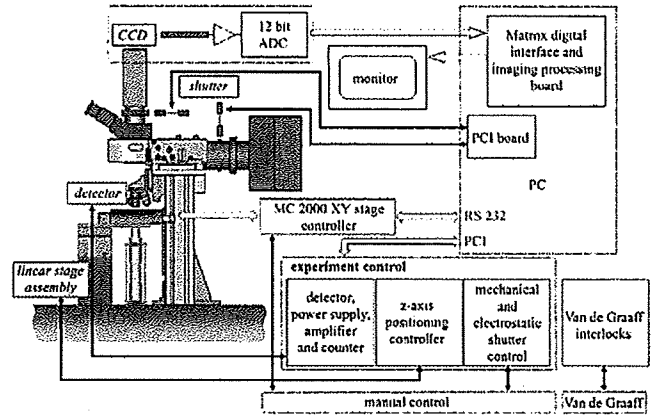

Fig. 18. A schematic diagram showing the overall controlling work of the CAS-LIBB microbeam facility.

performed by a microscope, a high-sensitivity CCD camera (CoolSnap HQ2, Photometrics, USA) and an image processing board using the Matrox Imaging Library in the computer. For the cell image processing, firstly the position of the microbeam exit is identified as the origin by the program. The fluorescent spot in the 18-μm thick scintillator excited by the traversing particles is used for this purpose. In cell irradiation, the auto-scanning sample stage (Märzhäuser, Wetzlar GmbH) locates cell by cell to the microbeam exit along a pre-calculated route. The number of the ions delivered to each cell is exactly controlled by the particle detector together with the electric beam-shutter (a pair of electrostatic deflecting plates). A home-developed program using Visual Basic under the Windows 2000 operating system integrates all these controlling work.[50)]

Performance of the microbeam facility

Quality of the collimated microbeam

The microbeam quality refers to the energy and spatial distribution of the collimated particles at the sample position. Simple adjustment of the inner beam parameters is not enough to get a high-quality microbeam extracted out. A high collimation level between the up-going beam from the second deflecting magnet and the collimator is necessary. After intensive and precautious adjustment of beamline components, a mono-energetic proton microbeam is stably acquired from the 1-μm collimator (Fig. 19). The normal energy of the microbeam is 2–3 MeV, with FWHM < 64.5 keV after the multi-layer detection system. The average counting rate is 1000–2000 cps. As for the spatial distribution, the etched pits on CR39 by the microbeam distributed within 5 μm diameter.

Particle detection and beam shutter

To shut off the beam after delivering a chosen number of ions to a cell, a reliable particle detector must be used. In our facility, the particles are detected by a transmission-type detector based on the 18 μm BC400 scintillator mounted bet-